

# Electric and magnetic resonances in arrays of coupled gold nanoparticle in-tandem pairs

Y. Ekinci<sup>1</sup>, A. Christ<sup>2</sup>, M. Agio<sup>3</sup>, O. J. F. Martin<sup>2</sup>, H. H. Solak<sup>4</sup>, and J. F. Löffler<sup>1</sup>

<sup>1</sup> Laboratory of Metal Physics and Technology, Department of Materials, ETH Zurich, 8093 Zurich, Switzerland

<sup>2</sup> Nanophotonics and Metrology Laboratory, EPF Lausanne, 1015 Lausanne, Switzerland

<sup>3</sup> Laboratory of Physical Chemistry, ETH Zurich, 8093 Zurich, Switzerland

<sup>4</sup> Laboratory for Micro- and Nanotechnology, Paul Scherrer Institute, 5232 Villigen-PSI, Switzerland

Corresponding author E-mail: [yasin.ekinci@mat.ethz.ch](mailto:yasin.ekinci@mat.ethz.ch)

**Abstract:** We present an experimental and theoretical study on the optical properties of arrays of gold nanoparticle in-tandem pairs (nanosandwiches). The well-ordered Au pairs with diameters down to 35 nm and separation distances down to 10 nm were fabricated using extreme ultraviolet (EUV) interference lithography. The strong near-field coupling of the nanoparticles leads to electric and magnetic resonances, which can be well reproduced by Finite-Difference Time-Domain (FDTD) calculations. The influence of the structural parameters, such as nanoparticle diameter and separation distance, on the hybridized modes is investigated. The energy and lifetimes of these modes are studied, providing valuable physical insight for the design of novel plasmonic structures and metamaterials.

©2008 Optical Society of America

**OCIS codes:** (160.3900) Metals; (160.4670) Materials: Optical materials; (260.2110) Physical optics: Electromagnetic optics

## References and links

1. C. F. Bohren and D. R. Huffman, *Absorption and Scattering of Light by Small Particles* (Wiley, 1983).
2. G. C. Schatz, R. P. Duyne, "Electromagnetic mechanism of surface enhanced spectroscopy," in *Handbook of Vibrational Spectroscopy*, J. M. Chalmers, P. R. Griffiths, eds., (John Wiley, 2002).
3. E. Ozbay, "Plasmonics: Merging photonics and electronics at nanoscale dimensions," *Science* **311**, 189-193, 2006
4. K. A. Willets and R. P. Van Duyne, "Localized surface plasmon resonance spectroscopy and sensing," *Annu. Rev. Phys. Chem.* **58**, 267 (2007).
5. M. Quinten and U. Kreibig, "Optical properties of aggregates of small metal particles," *Surf. Sci.* **172**, 557-577 (1986)
6. M. Moskovits, "Surface-enhanced spectroscopy," *Rev. Mod. Phys.* **57**, 783-828 (1985).
7. K.-H. Su, Q.-H. Wei, X. Zhang, J. J. Mock, D. R. Smith, and S. Schultz, "Interparticle coupling effects on plasmon resonances of nanogold particles," *Nano Lett.* **3**, 1087-1090 (2003).
8. T. Atay, J.-H. Song, and A. V. Nurmikko, "Strongly interacting plasmon nanoparticle pairs: From dipole-dipole interaction to conductively coupled regime," *Nano Lett.* **4**, 1627-1631 (2004).
9. C. Dahmen, B. Schmidt, and G. von Plessen, "Radiation damping in metal nanoparticle pairs," *Nano Lett.* **7**, 318-322 (2007).
10. W. Rechberger, A. Hohenau, A. Leitner, J. R. Krenn, B. Lamprecht, and F. R. Aussenegg, "Optical properties of two interacting gold nanoparticles," *Opt. Commun.* **220**, 137-141 (2003).
11. K. Kneipp, Y. Wang, H. Kneipp, L. T. Perelman, I. Itzkan, R. Dasari, and M. S. Feld, "Single molecule detection using surface-enhanced Raman scattering (SERS)," *Phys. Rev. Lett.* **78**, 1667-1670 (1997).
12. H. Xu, J. Aizpurua, M. Käll, and P. Apell, "Electromagnetic contributions to single-molecule sensitivity in surface-enhanced Raman scattering," *Phys. Rev. E* **62**, 4318-4324 (2000).
13. T. Pakizeh, M. S. Abrishamian, N. Granpayeh, A. Dmitriev, and M. Käll, "Magnetic-field enhancement in gold nanosandwiches," *Opt. Express* **14**, 8240-8246 (2006).
14. K.-H. Su, Q.-H. Wei, and X. Zhang, "Tunable and augmented plasmon resonances of Au/SiO<sub>2</sub>/Au nanodisks," *Appl. Phys. Lett.* **88**, 063118 (2006).
15. A. Dmitriev, T. Pakizeh, M. Käll, and D. S. Sutherland, "Gold-silica-gold nanosandwiches: tunable bimodal plasmonic resonators," *Small* **3**, 294-299 (2007).
16. P. Nordlander, C. Oubre, E. Prodan, K. Li, and M. I. Stockman, "Plasmon hybridization in nanoparticle dimers," *Nano Lett.* **4**, 899 (2004).

17. N. Feth, C. Enkrich, M. Wegener, and S. Linden, "Large-area magnetic metamaterials via compact interference lithography," *Opt. Express* **15**, 501-507 (2007).
18. H.-K. Yuan, K. C. Uday, W. Cai, A. V. Kildishev, A. Boltasseva, V. P. Drachev, and V. M. Shalaev, "A negative permeability material at red light," *Opt. Express* **15**, 1076-1082 (2007).
19. H. H. Solak, Y. Ekinci, P. Käser, and S. J. Park, "Photon-beam lithography reaches 12.5 nm half-pitch resolution," *Vac. Sci. Technol. B* **25**, 91-95 (2007).
20. Y. Ekinci, H. H. Solak, C. Padeste, J. Gobrecht, M. P. Stoykovich, and P. F. Nealey, "20 nm Line/Space Patterns in HSQ Fabricated by EUV Interference Lithography," *Microelectron. Eng.* **84**, 700-704 (2007).
21. A. Taflove and S. C. Hagness, *Computational Electrodynamics: The finite-difference time-domain method*, 3<sup>rd</sup> Edition (Artech House, 2005).
22. *CRC Handbook of Chemistry and Physics*, 87<sup>th</sup> Ed. (CRC Press, 2006).
23. C. Sonnichsen, T. Franzl, T. Wilk, G. von Plessen, and J. Feldmann, "Drastic reduction of plasmon damping in gold nanorods," *Phys. Rev. Lett.* **88**, 077402 (2002).
24. A. Wokaun, J. P. Gordon, and P. F. Liao, "Radiation damping in surface-enhanced Raman-scattering," *Phys. Rev. Lett.* **48**, 957 (1982).
25. C. L. Haynes, A. D. McFarland, L. Zhao, R. P. van Duyne, G. C. Schatz, L. Gunnarson, J. Prikulis, B. Kasemo, and M. Käll, "Nanoparticle optics: The importance of radiative dipole coupling in two-dimensional nanoparticle arrays," *J. Phys. Chem. B*, **107**, 7337-7342 (2003).
26. U. Fano, "Effects of configuration interaction on intensities and phase shifts," *Phys. Rev.* **124**, 1866 (1961).
27. S. Fan and J. D. Joannopoulos, "Analysis of guided resonances in photonic crystal slabs," *Phys. Rev. B* **65**, 235112 (2002).
28. C. Ropers, D. J. Park, G. Stibenz, G. Steinmeyer, J. Kim, D. S. Kim, and C. Lienau, "Femtosecond light transmission and subradiant damping in plasmonic crystals," *Phys. Rev. Lett.* **94**, 113901 (2005).
29. A. Christ, Y. Ekinci, H. H. Solak, N. A. Gippius, S. G. Tikhodeev, and O. J. F. Martin, "Controlling Fano interference in a plasmonic lattice," *Phys. Rev. B*, **76**, 201405(R) (2007).

## 1. Introduction

The optical properties of metal nanoparticles (NPs) are defined by their plasmon modes, which can be modified by the NP size, shape and background [1]. Tuning of such resonances offers many interesting applications, for instance in photonics and biosensing [2-4]. Further tailoring of plasmon modes can be achieved when NPs are brought into coupling. Earlier interest in the interaction of NPs was inspired by the significant effects of coupling on the averaged spectra of densely-deposited metal clusters and colloids [5, 6]. In the last decade, the coupling of closely-spaced NPs has been extensively investigated, supported by the broad availability of lithographic tools, which enable systematic studies of well-defined plasmonic structures [7, 8]. The most important consequence of coupling of two NPs is that the near-field between them is much stronger than that of an isolated NP, if the incident light is polarized along the NP center-to-center axis [7-10]. Such "in-plane" NP pairs might enable the detection of surface-enhanced Raman scattering down to the single-molecule level [11, 12].

Another route of plasmon coupling has been recently realized by metal-dielectric-metal nanosandwiches [13-14]. In this case the coupled pairs are aligned along the light propagation direction, which is termed as "end-fire" [13] or "in-tandem" configuration. When two NPs are brought into strong coupling, plasmon hybridization occurs and the initial degenerate plasmon modes split into two resonances: One is symmetric, i.e. the dipolar moments of the NPs are parallel, and the other one is antisymmetric, i.e. the dipolar moments are in opposite directions [13-16].

Unlike for in-plane coupling, where only the symmetric mode is accessible in far-field experiments, the antisymmetric mode of in-tandem NP pairs can also be excited. While the symmetric resonance has an electric dipolar character, the antisymmetric resonance generates a loop-like current in the NP pair and thus a dipolar magnetic moment [17-18]. An array of these "magnetic atoms" can exhibit an effective negative permeability and, therefore, this system has attracted significant attention, mainly in conjunction with metamaterials [17, 18].

A better understanding of the underlying physics of in-tandem NP pairs would be of high value for potential applications in the field of metamaterials and near-field enhanced spectroscopy. Thus, we have fabricated well-defined and large-area 2D arrays of in-tandem

NP pairs with different separations and NP diameters. The reflection and transmission spectra have been measured, providing complete information on far-field properties. Information on the near-field properties has also been obtained by extensive simulations based on the Finite-Difference Time-Domain (FDTD) method. The resonant energies and lifetimes of the hybridized plasmon modes have been analyzed and their dependence on structural parameters investigated. Finally, we have applied a Fano-type model to describe the optical spectra of in-tandem NP pairs, which provides further insight into the properties of coupled NPs.

## 2. Results and discussion

Ordered arrays of Au/MgF<sub>2</sub>/Au nanosandwiches with a small size distribution have been fabricated on quartz (high-purity fused silica, HPFS) substrates using EUV interference lithography. This method allows fabrication of periodic nanostructures with half-pitches down to 12.5 nm over large areas in extremely short exposure times [19]. The sample preparation started with spin-coating of a bilayer resist stack consisting of 100-nm-thick polymethylmethacrylate (PMMA) and 30-nm-thick hydrogen silsesquioxane (HSQ) layers on quartz wafers. EUV exposure, development of the HSQ photoresist in tetra-methyl ammonium hydroxide (TMAH) [20], and subsequent RIE etching with O<sub>2</sub> plasma resulted in hole patterns in the HSQ/PMMA bilayer with an undercut which facilitates a later lift-off process. E-beam-assisted evaporation of a 2-nm-thick Cr adhesion layer, Au, and MgF<sub>2</sub> was followed by the lift-off in acetone bath with ultrasonic agitation. SEM images of the resulting samples can be seen in Fig. 1.

The period of the NP arrays was fixed to  $p = 200$  nm by the grating mask used in the interference lithography. This subwavelength period ensures the absence of diffraction effects and a high signal level in the spectroscopic measurements due to the high density of the structures. The area of the arrays was 400×400 μm<sup>2</sup>. Both paired NP and single NP arrays were fabricated with diameters  $D$  ranging from 105 to 35 nm. Diameters were varied by changing the EUV exposure dose. The thickness  $t$  of the gold NPs was kept constant at 20 nm. The gap  $s$  between the NPs, which is defined by the thickness of the MgF<sub>2</sub> spacing layer, is chosen as 10 nm, 20 nm, and 35 nm, respectively, for each NP diameter with an accuracy of ± 2 nm. As seen in Fig. 1, the NP pairs have a conical shape as a result of self-shadowing of the films during evaporation. A schematic cross-section of the structures is shown in Fig. 1(d). By determining the top and bottom diameters of the structures, we obtained a best-fit angle of the conical shape as  $\theta = 12.5^\circ \pm 2^\circ$ .

In the following, we measured the transmission and reflection spectra of the samples using a microscope coupled to a spectrometer with a numerical aperture of 0.4 and a spot size of 100 μm. Figures 2(a) and 2(b) show the measured transmission and reflection spectra of the sample with a spacing layer thickness of 10 nm for various NP diameters ranging from 105 nm to 35 nm. The transmission spectra provide information on the total extinction, while the reflection spectra are related to the scattering processes. Thus we extracted the absorption spectra (see Fig. 2(c)) from the transmission and reflection spectra. This gives us information on the exact position of the resonances and allows us to separate scattering and absorption, which show quite different characteristics as seen in Figs. 2(b) and 2(c). Further discussion will be based on reflection and absorption spectra only.

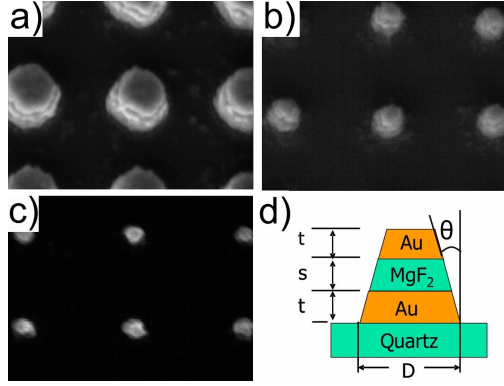


Fig. 1. SEM images of 2D arrays of Au NP pairs with diameters of (a) 105 nm; (b) 50 nm; and (c) 35 nm. The array period is 200 nm. (d) Schematic cross-section of Au NP pairs with a conical shape.

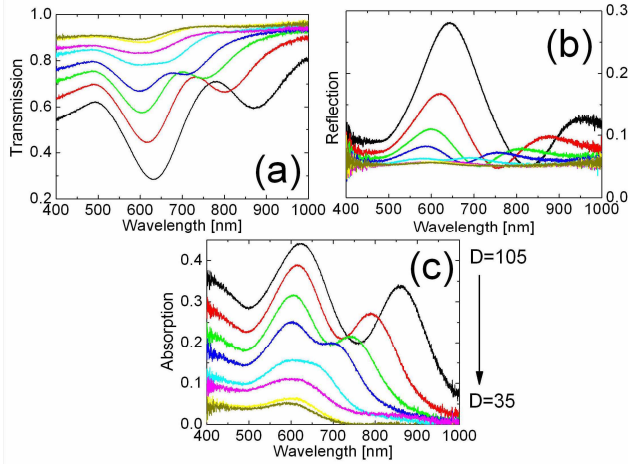


Fig. 2. Measured (a) transmission and (b) reflection spectra, and (c) extracted absorption spectra for Au NP pairs with diameters of  $D = 105, 87, 77, 70, 53, 46, 38$ , and  $35\text{ nm}$ . The array period is  $p = 200\text{ nm}$ ,  $s = 10\text{ nm}$ , and  $t = 20\text{ nm}$ .

The spectra in Fig. 2(c) display two resonances and their evolution with changing NP diameter. The peaks at shorter wavelengths are electrical dipolar (symmetric) resonances, whereas the long-wavelength peaks emerge from the magnetic dipolar (antisymmetric) resonances of the NP pairs, which will be confirmed by FDTD simulations below. With decreasing NP diameter all intensities decrease, but the decrease in the reflection spectra is more pronounced than in the absorption spectra. This is identical to the dipolar approximation of an isolated conducting spheroid, in which the extinction cross-section scales with the square of the diameter, while the scattering cross-section scales with the fourth power of the diameter [1]. The magnetic resonance shifts to the blue with decreasing NP diameter, while the electric resonance tends to be stationary. Note that the resonant wavelengths are also affected by the neighboring pairs due to radiative coupling, and therefore the period of the structure has also an effect. Nevertheless, the radiative coupling leads to relatively small shifts for the chosen array period [9] and the resonant energies are mainly defined by the structural parameters of the single pairs. Another interesting feature in Fig. 2 is the aforementioned significant difference between the absorption and reflection spectra. A comparison of the relative peak intensities in absorption and reflection spectra reveals that the antisymmetric

resonance is mainly absorptive, while the symmetric one exhibits strong scattering. Moreover, the magnetic resonance peaks in the reflection spectra are asymmetric and the peak positions are different from that in the absorption spectra. These differences highlight the importance of the absorption spectra for a detailed investigation of such hybrid structures.

Figure 3 shows the evolution of magnetic and electric resonances of in-tandem NP pair arrays with changing NP gap and for a fixed NP diameter of 105 nm. In the absorption spectra (Fig. 3(a)) we notice that with an increasing gap the magnetic resonance shifts to shorter wavelengths, whereas the effect of the gap distance on the position of the electric dipole mode is relatively small. In the reflection spectra (Fig. 3(b)), the magnetic resonance is relatively weak for a gap distance of 10 nm and becomes the dominant peak with an increasing gap.

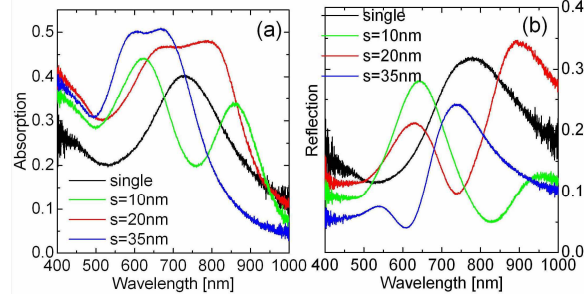


Fig. 3. Experimental (a) absorption and (b) reflection spectra of single NP arrays and paired NP arrays with gaps of  $s = 10, 20$ , and  $35$  nm;  $p = 200$  nm,  $D = 105$  nm, and  $t = 20$  nm.

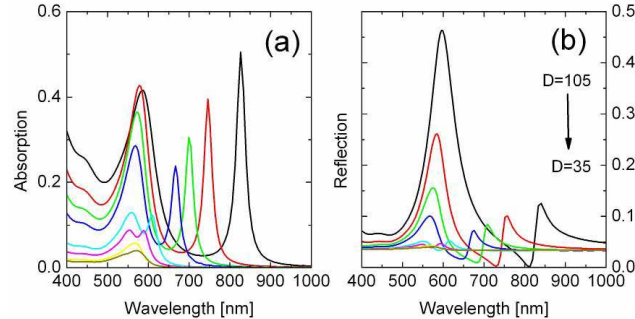


Fig. 4. Calculated (a) absorption and (b) reflection spectra of Au NP pair arrays with diameters of  $D = 105, 87, 77, 70, 53, 46, 38$ , and  $35$  nm;  $p = 200$  nm,  $s = 10$  nm, and  $t = 20$  nm.

For comparison and further analysis we performed Finite-Difference Time-Domain (FDTD) [21] simulations. The calculations are based on a Lorentz-Drude fit of the optical constants of Au [22] and the space discretization is set to 1 nm. Simulations are carried out for a unit cell of the array with periodic boundary conditions. Since the optical measurements are carried out with a numerical aperture of 0.4, in which about more than 90% of the illuminated power has a polarization parallel to the surface, assuming plane wave illumination in the calculations is a good approximation for comparison with the experimental results. Calculated absorption and reflection spectra for a NP gap of 10 nm and for various NP diameters are shown in Fig. 4, while the comparison with the measured spectra for two different distances  $s$  (and  $D = 105$  nm) is provided in Fig. 5. The overall agreement with the experiment in terms of peak positions is rather good, despite the fact that the peak positions are highly sensitive to the structural parameters. The major difference between the experiment and the theory is in the widths of the peaks, resulting from inhomogeneous broadening. This comes partly from

the NP size dispersion, which is found to be about 5% from an evaluation of the SEM images, and from the significant shape dispersion. Note that the present dimensions are about 100 nm and below. The finite crystallite size of gold results in arbitrary shapes instead of identical NPs with well-defined geometry. Moreover, the films have thicknesses down to 10 nm, making the relative roughness of the sandwiched layers significant. Further, the optical constants of the real structure can be different from the reported values of the bulk material.

Figure 6 displays the calculated field distributions near the Au NP pairs for both electric and magnetic resonances. The electric field is strongly enhanced at the sides of the NPs, indicating strong charge accumulations at these sites. The clear evidence of distinct magnetic and electric resonances can be seen in the phase distribution of the electric field. At the electric resonance (see Fig. 6(a)) the dipolar moments of both NPs are symmetric and oscillate in phase, while at the magnetic resonance (see Fig. 6(b)) the phase of the electric field is reversed by a factor of  $\pi$ , indicating that the dipolar moments of the individual NPs are opposite. The result of these in-phase and anti-phase dipolar moments can be seen in the magnetic field distributions. At the electric resonance the magnetic field between the NPs is nearly cancelled, whereas at the magnetic resonance the dipoles oscillating in anti-phase create a loop-like current which generates a strong magnetic field between the NPs.

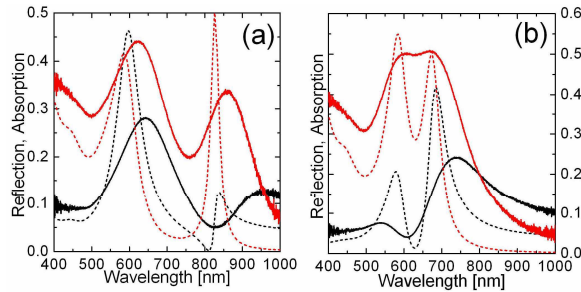


Fig. 5. Comparison of experimental and theoretical reflection and absorption spectra for paired Au NPs with (a)  $s = 10$  nm and (b)  $s = 35$  nm;  $p = 200$  nm,  $D = 105$  nm, and  $t = 20$  nm. The solid lines represent experimental data, while the dashed lines result from FDTD calculations. Black lines stand for reflection spectra and red lines denote absorption spectra.

Figure 7 shows the resonant peak positions as a function of NP diameter for various spacer layer thicknesses. The peak positions are extracted from the absorption spectra calculated by FDTD simulations, which do not suffer from inhomogeneous broadening and experimental uncertainties. The plasmon peak positions of single gold NPs are also shown as a function of the particle diameter, exhibiting red-shift due to retardation effects. For the paired NPs the magnetic dipolar resonance depends strongly on the geometrical parameters, which can also be seen in Figs. 2-4. The energy of the magnetic resonances (squares in Fig. 7) approaches that of the single NPs with decreasing NP diameter or increasing gap. On the other hand, the electric dipolar resonance (circles in Fig. 7) is rather insensitive to NP diameter and gap. In fact, the electric resonance has an energy similar to that of the plasmon resonance of single NP with double thickness (not shown). This can be understood as follows: in the symmetric (electric dipolar) resonance the NPs oscillate in phase. Since the separation between the NPs is much smaller than the wavelength, the in-phase resonance resembles the dipolar resonance of a single NP with double thickness. On the other hand, the antisymmetric resonance is created by breaking the geometrical symmetry and it requires a strong retardation of the total electric field. The field scattered by one NP induces an electric field on the other one, which is larger than the incident field and opposite in direction, so that the total electric field is reversed, i.e. retarded by 180 degrees as shown in Fig. 6(b). The induced field is inversely proportional to the separation and proportional to the polarizability of the NP, which scales

with the square of the diameter for an oblate NP. Therefore the energy and the oscillator strength of the magnetic resonance depend strongly on the geometrical parameters.

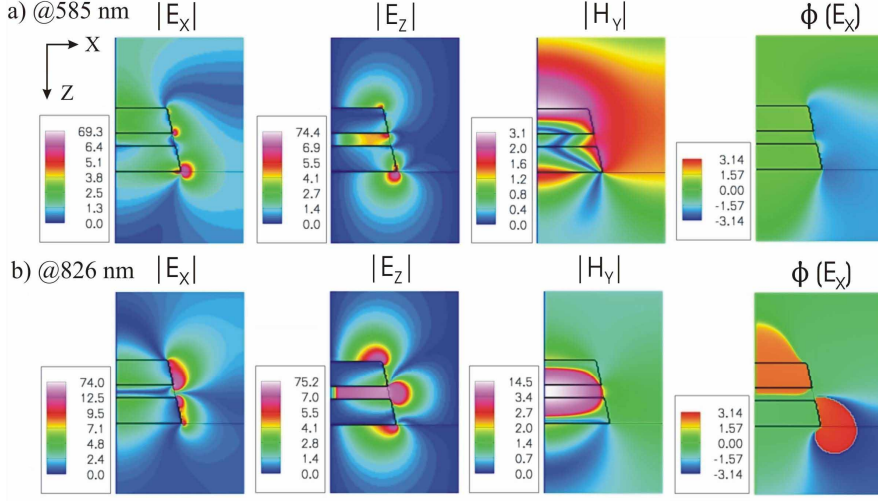


Fig. 6. Calculated electric and magnetic field enhancements ( $|E_x|$ ,  $|E_z|$ ,  $|H_y|$ ) and electric field phase distribution ( $\phi(E_x)$ ) in the vicinity of Au NP pairs (a) at the symmetric resonance ( $\lambda = 585$  nm) and (b) at the antisymmetric resonance ( $\lambda = 826$  nm);  $p = 200$  nm,  $s = 10$  nm, and  $t = 20$  nm. Incident field is polarized along the  $x$  axis.

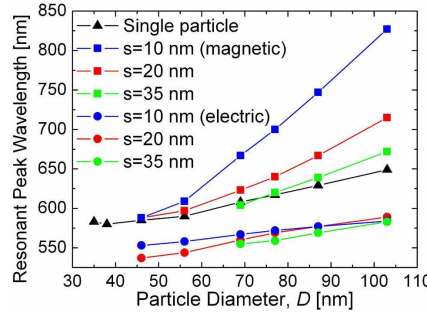


Fig. 7. Resonant peak positions for various gaps and NP diameters. Circles and squares denote symmetric and antisymmetric resonances, respectively. The single NP case is depicted with triangles.

Another important parameter of the resonances is their lifetime, which is plotted in Fig. 8 for both magnetic and electric modes as a function of resonance energy. The lifetimes ( $\tau = \hbar/I$ ) are extracted from the linewidths (FWHM =  $I$ ) of the peaks of the calculated absorption spectra. Since in some cases the magnetic and electric resonance peaks show a spectral overlap, only the lifetimes that can be extracted unambiguously by multiple-peak fitting are plotted. As seen in the figure, the resonance energies of the single NPs and the symmetric resonances of the NP pairs change with NP size, but the lifetime does not change significantly. However, the lifetime of the antisymmetric mode increases drastically with increasing NP diameter and decreasing gap. The increase in the lifetimes is as high as a factor of 4, which is partly due to the reduction in absorption since the resonance energies are red-shifted [23]. Further, even for the same energy, the lifetime increases with decreasing gap,

because the radiative rate decreases, resulting from the fact that the scattered fields of the opposing dipoles partly cancel out in the far-field. The longer lifetimes can be also explained by the reduced restoring force of the plasmon oscillations due to the strong interaction of opposite charges formed at the ends of the NPs. This occurs also for in-plane NP pairs, where opposite charges are formed across the gap for the longitudinal polarization in the symmetric resonance [9]. The smaller radiative rate favors a stronger field enhancement [9, 24], which can also be seen by comparing Figs. 6(a) and 6(b).

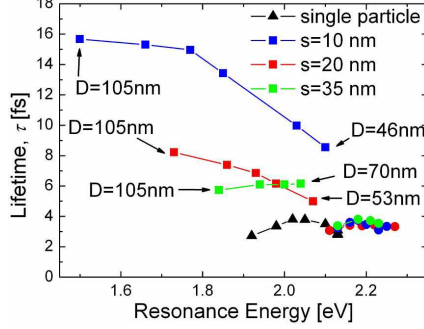


Fig. 8. Lifetime and resonance energy of the plasmon modes for various NP gaps and diameters. Circles and squares denote symmetric and antisymmetric resonances, respectively; triangles stand for single NP arrays. The symbols for a certain gap value are connected with lines. The corresponding NP diameters are provided at the ends of the curves.

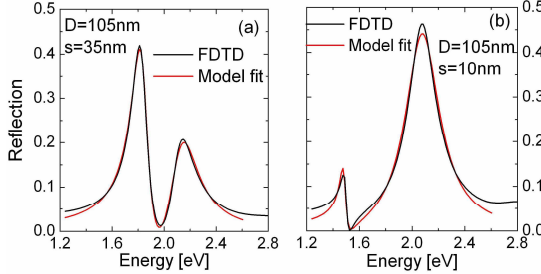


Fig. 9. FDTD calculated reflection spectra (black) and best-fit curves (red) using a Fano-type model for paired Au NP arrays with (a)  $s = 35\text{ nm}$  and  $D = 105\text{ nm}$ , and (b)  $s = 10\text{ nm}$  and  $D = 105\text{ nm}$ . The best-fit parameters for (a) are  $a = 0.024$ ,  $b_a = 0.71$ ,  $\varphi_a = 0.32\pi$ ,  $\Gamma_a = 78\text{ meV}$ ,  $E_a = 1.84\text{ eV}$ ,  $b_s = 0.54$ ,  $\varphi_s = 0$ ,  $\Gamma_s = 139\text{ meV}$ , and  $E_s = 2.11\text{ eV}$ ; and for (b) are  $a = 0.002$ ,  $b_a = 0.33$ ,  $\varphi_a = 0.15\pi$ ,  $\Gamma_a = 28\text{ meV}$ ,  $E_a = 1.49\text{ eV}$ ,  $b_s = 0.67$ ,  $\varphi_s = 0$ ,  $\Gamma_s = 160\text{ meV}$ , and  $E_s = 2.08\text{ eV}$ .

It should be noted that in the present study, in which the influence of the structural parameters on the energy and lifetimes of the modes is analyzed, the periodicity of the structure is fixed. The radiative interaction between the nanoparticles of the array has some effect on the energy and lifetime of the nanoparticle pairs. However this interaction is relatively weak compared to the near-field interaction between the coupled nanoparticles of the pairs for the chosen structural parameters [7, 9, 10, 25]. Therefore, the energy and lifetime of a single and isolated pair will only be slightly different from those of the pairs in a periodic array or in a random ensemble.

One remarkable feature of the measured and calculated reflection spectra is that the line shapes of the magnetic resonance are highly asymmetric. Such asymmetry emerges from the spectral interference of the two resonances with the continuum background and is referred as

Fano lineshape [26], which has also been reported in photonic and plasmonic crystals [27-29]. The Fano lineshapes of the far-field reflection amplitude  $R(\omega)$  can be described as [27-29]

$$R(\omega) = |r(\omega)|^2 = \left| a_r + \sum_{j=s,a} \frac{-b_j \Gamma_j e^{i\varphi_j}}{\hbar\omega - E_j + i\Gamma_j} \right|^2, \quad (1)$$

where the complex scattering function  $r(\omega)$  is the sum of a constant background  $a_r$  and the symmetric and antisymmetric eigenmodes parameterized by their amplitude  $b_j$ , phase  $\varphi_j$ , linewidth  $\Gamma_j$  and energy  $E_j$ . Best-fit curves of this phenomenological model to the spectra obtained by FDTD calculations are shown in Fig. 9. The best-fit parameters are given in the figure caption. This model not only provides a good fit to the calculated spectra, but also delivers insightful information on oscillator strengths, linewidths and energies of the resonances from the reflection spectra. In addition, one can extract the relative phases of the modes, which would otherwise not be possible.

### 3. Conclusions

In summary, we have analyzed the coupling behavior and the resonances of arrays of in-tandem Au NP pairs. The coupling leads to two eigenmodes: one is symmetric, electric dipolar and superradiant; the other one is antisymmetric, magnetic dipolar and subradiant. A phenomenological Fano model provides physical insight into, e.g., relative phase and oscillator strengths of the eigenmodes. In-tandem pairs are highly tunable systems in which resonance energy, lifetime, and near-fields can be easily tailored. The prolonged lifetime of the magnetic mode is of great interest, since the typical lifetimes of the localized plasmon modes are in the femtosecond range. Thus, in-tandem pairs with long lifetimes might be useful in applications where long coherent interaction times are required. We showed that the energy and lifetime of the magnetic resonances are highly sensitive to the structural parameters, which offers interesting opportunities in the context of metamaterials and plasmonic device design. Another important application of in-tandem pairs would be in plasmon-enhanced spectroscopy. For instance, in Raman spectroscopy with large Stokes or anti-Stokes shifts, or in fluorescence spectroscopy, the existence of two tunable plasmon resonances should enable stronger signal enhancements.

### Acknowledgments

This work was supported by the ETH Zurich Initiative on Composite Doped Metamaterials (CDM) and by ETH Research Grant TH-29/07-3. MA thanks Vahid Sandoghdar for continuous support and encouragement. AC and OJFM gratefully acknowledge funding from the European Commission (contract Nr. IST FP6-202-IST-1-507879) and from the Swiss National Science Foundation (contract Nr. R'Equip 206021). Part of this work was performed at the Swiss Light Source (SLS), Paul Scherrer Institute, Switzerland.